Research Article

Merdin Danışmaz*, and Mesut Demirbilek

Assessment of heat transfer capabilities of some known nanofluids under turbulent flow conditions in a five-turn spiral pipe flow

https://doi.org/10.1515/arh-2024-0002
received January 24, 2024; accepted February 29, 2024

Abstract: In this study, the thermo-flow behaviours of the spiral tube were examined using water and some nanofluids such as TiO_2, Al_2O_3, Fe_2O_3, CuO, ZnO, and CeO_2. The computational flow dynamic modelling of the spiral coiled tube was performed with ANSYS 20 software program. The k–ε model with a standard wall function was used to simulate the thermo-flow characteristics. The solution of the governing equations was performed using the discretization method of finite volume. The study was carried out considering the case of fluid-to-fluid heat transfer in turbulent conditions. The influence of different key design parameters such as Reynolds number, different nanofluids, and flow arrangements was of main interest. The volume concentration of the nanofluids is 1%. The experiments were performed at different Reynolds ranges (9,000, 14,000, 20,000, and 25,000). The outlet temperature values, heat transfer coefficient, coefficient of friction, Nusselt number values of water, and nanofluids were found and compared. It was found that the outlet temperature, heat transfer coefficient, and Nusselt number values of water were the lowest, while the coefficient of friction value was the highest compared to the nanofluids. Among the nanofluids, CeO was found to have the highest outlet temperature, heat transfer coefficient, and Nusselt number value, as well as the lowest coefficient of friction value. TiO_2 was found to have the lowest outlet temperature (T_{out}), the heat transfer coefficient value, and the highest coefficient of friction value. Al_2O_3 was found to have the lowest Nusselt number. In addition, Nusselt number values were obtained at different Dean numbers of water (2,200, 3,400, 4,900, 6,100, 7,350, and 8,600) and found to be compatible with previous studies. In addition, the coefficients of friction values of water at different velocities (0.18, 0.24, 0.41, 0.71, 0.95, 1.07, and 1.18) were obtained and found to be compatible with previous studies.

Keywords: spiral tube, nanofluid, Nusselt number, fluid flow, CFD

1 Introduction

In a variety of engineering applications, including power plants, chemical reactions, air conditioning, refrigeration, food processing, rocket engines, and waste heat system recuperation, heat exchange devices are frequently utilized. Heat transfer tubes are frequently used in these heat exchange devices. Spiral tubes, which offer greater heat transmission in a smaller volume, can also be used and rearranged to enhance heat transfer in addition to finned surfaces. Providing increased surface area for a given volume (tightness) and the benefits of the centrifugal force that results from fluid movement in spiral tubes are the key advantages of utilizing spiral tubes. By inducing a secondary flow dependent on the pipe curvature ratio, this centrifugal force enhances the heat transmission qualities in comparison to a straight pipe. Ciofa et al. [1] examined the effects of centrifugal buoyancy and gravity on heat transfer in circular and helical tubes as well as laminar pipe flow numerically. They found that in helical tubes, positive centrifugal and gravitational buoyancy quantities result in the lowest friction factor and Nu values. They found that when centrifugal buoyancy and gravity are both negative, the friction factor and Nu values are at their maximum. Additionally, they discovered that in annular tubes, gravitational buoyancy had no discernible impact on the friction factor or Nu, but both dropped with increasing centrifugal buoyancy intensity. A numerical investigation of the impact of secondary flow on heat transfer in spiral (bent) tubes was conducted by Nobari and Amani [2]. They consequently discovered that the

*** Corresponding author: Merdin Danışmaz,** Department of Mechanical Engineering, Kırşehir Ahi Evran University, Kırşehir, Turkey, e-mail: m.danismaz@ahievran.edu.tr
Mesut Demirbilek: Department of Mechanical Engineering, Kırşehir Ahi Evran University, Kırşehir, Turkey

centrifugal force acts on the pipe's input region, causing the maximum velocity to shift from the pipe's centre to its outside wall. The heat transfer characteristics of coiled tubes in relation to single-phase flow were determined by Wang et al. [3]. They examined how buoyancy and centrifugal force affected the heat transfer coefficients. They calculated a non-dimensional number that positioned between buoyancy and centrifugal force to predict the heat transfer characteristics in a helical tube. Al_2O_3 and CuO nanofluids were evaluated [4] in a spiral tube as working fluids with various curvature ratios. The authors consequently discovered that as the concentration of the nanofluid increased, the heat transmission increased, and the curvature ratio decreased. In order to design spiral tube heat exchangers, Patil [5] examined the heat transfer in spiral tubes in the laminar flow area of Newtonian fluids and created new correlations. An enhanced modelling technique for accurate fouling thickness and milk outflow temperature prediction was developed by Nema and Datta [6]. They consequently found that, over time, fouling increases and the outlet temperature decreases.

The performance characteristics of spiral tubes and elliptical cross sections were studied numerically by Ji et al. [7]. They discussed the impact of pitch, curvature ratio, mass flow rates, and structural characteristics. They discovered that when the water mass flow rate or helical inclination increases, so does the amount of heat transmission. A novel design for a cylindrical hollow chamber receiver was examined experimentally [8]. In order to attain optimal efficiency, they studied the impact of the effective aperture area based on the hollow chamber length and the number of cycles. Hardik et al. [9] conducted research on the local heat transfer coefficient in a coiled tube with water flow. Consequently, they proposed the secondary average local Nu and the average Nu cooperation for the entire tube.

After studying the developed flow in a helical tube, Kim et al. [10] introduced a novel type of correlation for various angles of the fully evolved flow. The air-side heat transfer properties of spiral-type circular finned tube heat exchangers, which are employed as evaporators in residential refrigerators, were examined by Lee et al. [11]. Both active and passive strategies were used to improve heat transport to thermal devices in an effort to raise their thermal efficiency. While the presence of external force is the prominent feature of the active method, changing the geometry and thermo-physical properties of the fluid by enhancing the base fluid with additions is an example of a passive method. Nanofluids contain chemically stable metals, such as copper and silver, metal oxides, such as alumina and bismuth oxide, and various carbon allotropes with higher thermal conductivity than the base fluids and significantly smaller than 100 nm in size. Modification of the transport and flow properties of the working fluid, application of nanoparticle doping in the base fluid, different curvature ratios, use of different nanofluids, pulsating flow, magnetic field, tube material, fluid flow type, geometry type, cross-section type, fluid velocity, and properties of the working fluid have been widely studied in the literature as techniques to increase heat transfer in spirally wound tubes. In a comprehensive study, Li et al. [12] investigated the thermo-fluid properties of propane condensation in spiral tubes. They developed the computational model based on the two-fluid multiphase model. They provided some guidelines for understanding the thermo-fluid properties of condensation in a spiral tube. Bartwal et al. [13] investigated the thermo-fluid flow properties of a meshed circular ring integrated in a smooth-flow circular tube. They found new empirical correlations between the Nusselt number and friction factor experimentally and numerically, which were in agreement with the experimental data. An examination of TiO_2–water nanofluid was employed by Eiamsa Ard et al. [14] to enhance the heat transfer flow in a hollow tube with twisted band joints. Consequently, they discovered that utilizing the nanofluid at a concentration of 0.15% by volume and a dimple angle of 45° produced the maximum thermo-hydraulic performance of 1.26. With redesigned helical–helical inserts, Verma et al. [15] enhanced the heat transmission and friction losses in the heat exchanger tube. They conducted tests on three different types of tubes: one with helical–helical inserts, one without, and three with modified helical–helical inserts. They correlated the empirical correlations of the Nusselt number and friction factor for helical–helical inserts. In order to study the heat transfer of convective nanofluids in vertical helically coiled tubes with varying shapes and uniform wall temperatures, Akhavan-Behabadi et al. [16] conducted experiments. They examined how the heat transfer and flow characteristics of the coolant passing through the tube were affected by the Reynolds number, Dean number, geometrical factors, and weight fractions of nanofluids. Narrein and Mohammed [17] examined the consequences of nanofluids on heat transfer and fluid flow properties in a helical-coiled tube heat exchanger and its rotation. The heat transfer and friction factor of CuO and Al_2O_3 nanofluids moving in a spiral pipe under boundary conditions of constant wall temperature were experimentally examined [18]. As working fluids, they employed nanofluids with volume concentrations of 0.55, 1.12, and 2.23%. They discovered that using nanofluids at higher concentrations produced noticeably higher Nusselt numbers and that there was very no pressure drop penalty

as the concentration of nanoparticles increased. In order to analyse the Nusselt number and friction factor of a vibrating nanofluid passing through a grooved tube with a magnetic field effect, Naphon et al. [19] used a novel adaptive inference system. In a similar study [20], the authors experimentally investigated the effect of heat transfer and friction factor properties of water and CuO in straight and helical dimpled tubes under turbulent flow conditions. They found that the Nusselt number with the dimpled tube was greater than the Nusselt number obtained with the straight tube, and the pressure loss of the nanofluids slightly increased compared to that of the distilled water. Sasmito et al. [21] conducted a quantitative investigation of CuO and Al_2O_3 nanofluid laminar flow in square cross-sectional tubes (straight, conical spiral, in-plane spiral, and helical spiral). The heat transfer and pressure drop properties of water-based copper oxide nanofluids in a helically wound heat exchanger were compared in an experimental work [22]. They consequently discovered that there was no distinction between horizontal and vertical configurations. Additionally, they suggested two relationships between the friction factor and the Nusselt number. Hashemi and Akhavan-Behabadi [23] investigated the pressure drop and heat transfer properties of oil and copper oxide in a horizontal helically wound tube under constant heat flux boundary conditions. They found that nanofluids have better heat transfer properties when they flow in a helical tube instead of a straight tube. They also proposed a new correlation for the Nusselt number. Jamshidi et al. [24] investigated the laminar heat transfer and pressure drop of some nanofluids that contained Al particles with volume concentrations of 1 and 2% inside the helical coils. A few studies [25,26] assessed how an agitated helical coil and flat heat exchanger performed in relation to the concentration of Al_2O_3 nanofluid. The impact of coil core and curvature ratio on the development of heat transfer in nanofluids and helical coils was assessed in some studies [27,28]. As working fluids, they employed carbon nanotubes and water at weight concentrations of 0.1, 0.3, and 0.5%. Khairul et al. [29] studied the effects of fluids such as water, CuO, Al_2O_3, and ZnO nanoparticles with volume concentrations ranging from 1 to 4% on the heat coefficient of transfer and entropy generation rate of helical-wrapped heat exchangers. The variables included were volume flow rate, mass flow rate, density, thermal conductivity, Reynolds number, and Nusselt number. The heat transfer performance of a flat spiral tube with various cross-sections, including circular, square, rectangular, triangular, trapezoidal, and semi-circular, was determined numerically [30]. The authors calculated Re at a constant value and the cross-sectional area. Boundary conditions included constant wall temperature and continuous heat flux. Consequently, they discovered that some sections – rectangular and otherwise – perform better than others in terms of heat transfer. Through computer modelling, Rahman et al. [31] investigated the forced convective heat transfer on the Al_2O_3–Cu/water hybrid nanofluid. They consequently found that the heat transfer coefficient increased as the volume concentration and Reynolds number of the hybrid nanoparticle increased in base fluids. Xuan and Lee [32] investigated the effect of the addition of nanoparticles on heat transfer enhancement. They found that the nanofluid has the potential to increase the heat transfer rate. Sheikholeslami et al. [33] numerically simulated the effects of magnetic force and radiation on nanofluid transport in a permeable medium considering Al_2O_3 nanoparticles. They found that convection decreases with increasing magnetic forces. The heat transfer of nanofluid flow in coiled tubes with constant heat flux was studied by Mirfendereski et al. [34]. They discovered that applying nanofluid to coiled tubing with increasing curvature increases heat transfer and decreases pressure loss more than when using a regular liquid (without any additions). The curvature effect, nanofluid density and hot fluid temperature, nanofluid heat transfer performance, and pressure drop parameters were considered. They found that for different nanofluid densities, Nu and friction factor were larger than water. The heat transfer characteristics of water–Al_2O_3 and water–CuO were studied by Nassan et al. [35] while taking laminar fluid flow and square-section pipe into consideration. They discovered that utilizing nanofluid increases heat transmission more than water and that the improvement in water–CuO (in square tubes) is higher. The nanofluid Al_2O_3/water was studied numerically [36] in an elliptical tube equipped with twisted tape. Consequently, they discovered that simultaneous use of the nanofluid and twisted tape improves thermal efficiency and heat transfer more than the separate applications of the nanofluid or twisted tape. Furthermore, Yoo et al. [37] numerically investigated the flow characteristics of spirally wound tubes using the ANSYS commercial program. They evaluated different geometries with various Reynolds numbers. They found that the Reynolds number-dependent Nu and friction factor have a more powerful influence in contrast to the curvature ratio of spirally coiled tubes. Malviya et al. [38] performed thermal and dynamic analyses for different bends of the spiral coil and conducted experiments to test the modified absorber. They found that the experimental results agree with the numerical results for the spiral absorber. Beigzadeh and Rahimi [39] predicted the hydrodynamic and heat transfer properties in coiled tubing by using the power of genetic algorithm-

based correlations and the adaptive neuro-fuzzy inference system. They made use of pressure drop and heat transfer experimental data from spiral tubes with various coil and pitch geometries. The coiled tubes were filled with hot water for the trials. Consequently, they discovered that, for Nu and f prediction, the mean relative errors of fuzzy models are 6.24 and 3.54%, respectively, whereas the mean relative errors of generic algorithm models are 8.06 and 5.03%, respectively. Seyedashraf [40] numerically simulated four spiral helical tubes with different curvature ratios under the condition of constant wall temperature to investigate their flow characteristics in terms of secondary flow and pressure drop and compared them with experimental data reported in the literature. He found that the experimental data and the results of this study are in agreement and proposed a novel connection to predict the pressure drop. Abdi et al. [41] performed a numerical analysis on the heat transfer performance at different Reynolds numbers in laminar flow of water/Al_2O_3 nanofluid at volume fractions of 0.1–0.7 in straight, spiral, and helical coiled tubes in varying cross-sectional areas such as circular and triangular. They found that the greatest heat transfer was in the rectangular tube, and the average heat transfer coefficient in the helically coiled tube was higher than that in the spiral and straight. They also found that the ratio of heat transfer to pressure drop was lower for helical–helical geometry than for spiral and straight geometry. Additionally, to investigate the heat transfer and flow properties of conventional fluids and nanofluids in spiral wound tubes, helical tubes, and tubes of other geometries, Huminic and Huminic [42] conducted a study that included experimental, numerical, and analytical research.

The importance of simple and compact designs in practical heat transfer applications is increasing day by day. Spiral tube heating is one of the standard pipe flow applications that fulfil this need. From the information and findings obtained from the literature survey, it is clear that the heat transfer in the spiral tube is open to improvement with the use of different nanofluids to improve heat conduction. Therefore, it is useful to study different nanofluids for a given spiral geometry and determine their contribution to improving heat transfer. This work includes the study of such an evaluation. From the previous studies given above, it is understood that passive arrangements for in-pipe flow and nanofluid flow significantly improve heat transfer. However, the utilization of nanofluids in spiral tube flow arrangements, which offer a compact heat transfer mechanism for small volumes, is a subject for further development. It is especially important to demonstrate the performance of some widely used nanofluids in such a system. This study investigates the thermal performances of nanofluid flows in compact spiral tube flow by numerical calculations. Studies such as this one, which provide high thermal performance in small volumes, remain up to date.

2 Numerical modelling and governing equations

2.1 Geometry

Ansys 2020 R2 was used to obtain the heat transfer behaviour of the spiral tube. To investigate the spiral tube's thermo-fluid characteristics, a 3D CFD model was created. In each cell, the governing equations for temperature, pressure, and fluid motion were solved. Modelling and analysis occurred in three steps. The first step in problem-solving is determining the spiral tube's geometry, which was accomplished using the SolidWorks 2023 drawing module (design modeller). Mesh generation was done in the next step with Ansys CFD. Model solving was suggested in the last phase using Ansys Fluent software. The geometry of the spiral tube is shown in Figure 1, where R_i is the innermost radius of the spiral tube, R_o is the outermost radius of the spiral tube, and p stands for the pitch of the spiral tube (distance between every two turns).

The flow methodology centres on the study of heat transfer at a constant surface temperature in a geometrical model representing spiral tube flow. Water and different water-based nanofluids enter the flow region at a uniform constant velocity and leave the geometry through the outlet region at the pressure outlet condition, realizing an internal flow with five full-turn rotations. Unlike standard planar internal flow, spiral tube flow also considers the effect of centrifugal forces on the flow region. This helps to improve the heat transfer. However, it is taken into account that nanofluids, which have better heat transfer properties than water, will provide additional thermal improvements. Generation of the average heat convection coefficient near the surfaces of the model and calculation of the average Nu number at the outlet take the lead in evaluating the improvements made.

Table 1 provides specific data on the spiral tube's geometrical parameters and simulation settings. The fluid in the spiral tube enters the inlet region and exits at the outlet region, as shown in Figure 1.

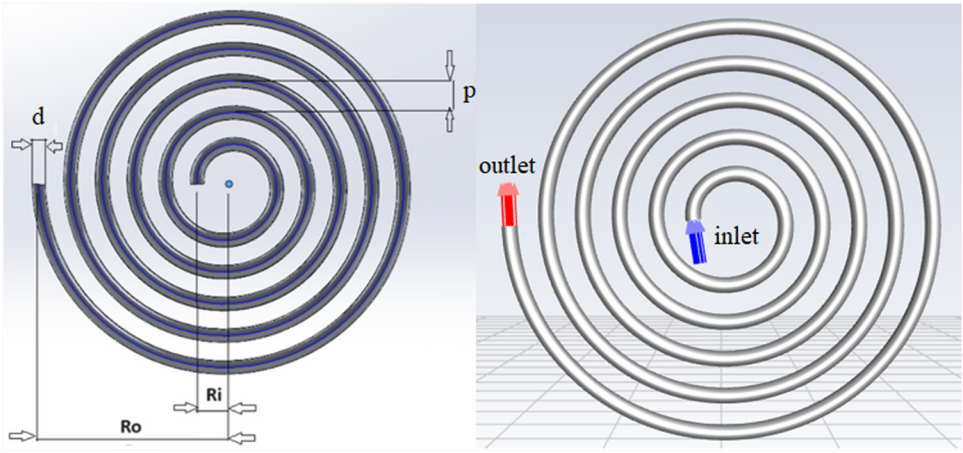

Figure 1: Geometry of the spiral pipe.

Table 1: Characteristics of the flow model

Properties	Value
Pipe diameter, d (mm)	8.5
Inside radius, R_i (mm)	20
Outermost radius, R_o (mm)	240
Length of the spiral helix, L (mm)	2201.87
Spiral helix pitch, p (mm)	20
Curvature ratio, δ	0.06
Number of helical turns, n	5
Fluid inlet temperature, T (°C)	20

2.2 Governing equations and data reduction

The evaluation of the volumetric concentration, together with the change of the base fluid and nanoparticles during the development of nanofluid, is a much studied situation and was detailed in the literature introduction. In this study, the base fluid is considered as water. By mixing nanoparticles with different properties, a nanofluid with new basic properties was determined. The density of the nanofluid ρ_{nf} depends on the density of the base fluid ρ_w, the density of the nanoparticle ρ_p, and the volumetric concentration ϕ, and is calculated using equation (1) [4,30].

$$\rho_{nf} = \phi\rho_p + (1 - \phi)\rho_w. \quad (1)$$

The specific heat of the nanofluid is related to the specific heat of the base fluid, the specific heat of the nanoparticle, and the volumetric concentration and is obtained from equation (2) [21–24]. Here, $(\rho C_p)_{nf}$ is the heat capacity of the nanofluids, $(\rho C_p)_w$ is the heat capacity of the base fluid, and $(\rho C_p)_p$ is the heat capacity of the nanoparticles:

$$(\rho C_p)_{nf} = \phi(\rho C_p)_p + (1 - \phi)(\rho C_p)_w. \quad (2)$$

The Drew and Passman Equations are proposed as the well-known equations for the calculation of viscosity, applicable to spherical particles with volume fractions less than 5.0% by volume, and is defined as follows [21–25].

$$\mu_{nf} = (1 + 2.5\phi)\mu_w. \quad (3)$$

Here, μ_{nf} is the viscosity of the nanofluids and μ_w is the viscosity of the base fluid.

The thermal conductivity of nanofluids was calculated using the following equation from Maxwell and Passman in the literature [21–25]:

$$k_{nf} = \frac{k_p + 2k_w - 2\phi(k_w - k_p)}{k_p + 2k_w + \phi(k_w - k_p)}k_w. \quad (4)$$

Here, k_{nf} is the thermal conductivity of the nanofluids, k_w is the thermal conductivity of the base fluid, and k_p is the thermal conductivity of the nanoparticles. The properties of the nanoparticles determined for the nanofluids used in this study are given in Table 2. Three different volumetric concentrations of nanofluids, 1, 3, and 5%, were developed and included in the analysis. These nanoparticles were specifically chosen because they are some of the most widely studied nanofluids in the literature.

Table 2: Nanoparticle properties

Nanoparticle	ρ (kg/m^3)	Cp (J/kg K)	k (W/m K)	Ref.
TiO_2	4,260	683–692	4.8–11.8	[4]
Al_2O_3	3,900	880	42.36	[43]
Fe_2O_3	5,420	628.30	13.55	[44]
CeO_2	7,132	460	12	[45]
CuO	6,530	540	18	[46]
ZnO	5,460	495.2	27.73	[44]

Different methods can be used for the basic conservation equations of mass, momentum, and energy. In this study, The realized k–ε model is used to model the thermo-flow characteristics of the spiral tube. The turbulent heat transfer flow characteristics of the spiral tube are shown in the tensor form [47,48].

Continuity equation:

$$\frac{\partial u_i}{\partial x_i} = 0. \tag{5}$$

Momentum equation:

$$\frac{\partial}{\partial x_j}\left[(\mu + \mu_t)\left(\frac{\partial u_i}{\partial x_j} + \frac{\partial u_j}{\partial x_i} - \delta_{ij}\frac{2}{3}\frac{\partial u_k}{\partial x_k}\right) - \rho u_j u_i - \delta_{ij} p\right] = 0. \tag{6}$$

Energy equation:

$$\frac{\partial}{\partial x_j}\left[\left(k + \frac{\mu_t C_p}{\sigma_t}\right)\frac{\partial T}{\partial x_j} - \rho u_j C_p T - \mu_l \frac{\partial u_i}{\partial x_j}\left(\frac{\partial u_i}{\partial x_j} + \frac{\partial u_j}{\partial x_i} - \delta_{ij}\frac{2}{3}\frac{\partial u_k}{\partial x_k}\right) + \rho\varepsilon\right] = 0. \tag{7}$$

The subsequent dimensionless parameters are presented to illustrate the thermo-fluid properties of the spiral tube. Dimensionless parameters such as Reynolds number, Dean number, curvature ratio, and Prandtl number, which add characteristic features to the flow, are determined as follows, respectively:

$$\mathrm{Re} = \frac{\rho v d}{\mu}, \mathrm{Dn} = \mathrm{Re}\,\delta^{1/2}, \delta = \frac{d}{R_i + R_o}, \mathrm{Pr} = \frac{C_p \mu}{k}, \tag{8}$$

where Re is the Reynolds number, ρ is the density, v is the velocity, d is the diameter, μ is the dynamic viscosity, Dn is the Dean number, δ is the curvature ratio, R_i is the inner radius, R_o is the outer radius, Pr is the Prandtl number, C_p is the specific heat, and k is the heat transfer coefficient.

The equations that drive the analysis are given in reduced form in the literature [40,43] and are expressed individually below.

The following equation is used to calculate how much heat is transferred from the fluid:

$$\dot{Q} = \dot{m} C_p (T_i - T_o), \tag{9}$$

where $\dot{Q}$ is the entire amount of heat transferred to the fluid along the flow, $\dot{m}$ is the mass flow rate of the fluid, and T_i and T_o are the inlet and outlet temperatures of the fluid, respectively.

The convective heat transfer coefficient for the system is given as follows:

$$h = \frac{\dot{Q}}{A\,\Delta T_{\mathrm{LMDT}}}, \tag{10}$$

where h is the average heat transfer coefficient, and A is the internal surface area of the spiral coiled tube. ΔT_{LMTD} is the logarithmic mean temperature difference and can be obtained from equation (11). Note that T_w is the wall temperature of the spiral tube.

$$\Delta T_{\mathrm{LMTD}} = \frac{(T_w - T_i) - (T_w - T_o)}{\mathrm{In}\left(\frac{(T_w - T_o)}{(T_w - T_o)}\right)}. \tag{11}$$

The Nusselt number (Nu) in the spiral tube fluid flow and the Darcy friction factor (f) in the inner ring hot fluid of the spiral tube are two important parameters used for the thermal assessment of the flow and are given in equations (12) and (13), respectively. Note that the pressure drop across the flow is determined as Δp and the characteristic length L:

$$\mathrm{Nu} = \frac{hd}{k}, \tag{12}$$

$$f = \frac{2\Delta p d}{\rho v^2 L}. \tag{13}$$

2.3 Boundary conditions

A non-slip boundary condition was installed on the spiral pipe's wall. Uniform profiles are employed for all of the fluid's dependent variables at the flow inlet. At the outlet, diffusion flows are set to 0 for all variables in the downstream direction. These expressions are defined in equations (14) and (15), respectively:

$$u = u_o, \quad T = T_o, \quad k = k_o, \quad \varepsilon = \varepsilon_o, \tag{14}$$

$$\frac{\partial}{\partial n}(u_i, T, k, \varepsilon) = 0. \tag{15}$$

2.4 Numerical procedure and mesh-independent test

A 3D geometric model representing the spiral pipe flow was created, and the details are given in the geometry section. We use the finite volume decomposition approach to solve the governing equations. The heat transfer and flow characteristics of the spiral tube with increasing

wall temperatures are studied using a realized k–ε turbulent viscous model. Conjugated heat transfer involving convection–conduction together is investigated through the area of a spiral tube. One proposed solution model for the pressure–velocity coupling approach is a discretized solver, which is the SIMPLEC-consistent algorithm [4]. The standard scheme is used in pressure discretization. A second-order upwind scheme is used to solve both momentum and energy equations. Convergence criteria of 10^{-4} for the continuity and momentum equations and 10^{-6} for the energy analysis were determined. Regardless of the number of runs, the analysis was terminated when these criteria were met. A tenth-generation computer with 12 cores and 32 GB memory was used for the analysis.

Figure 2 shows the mesh generation process of the spiral pipe in the finite element model. It is important to determine that the solution is independent of the number of cells or nodes or that a sufficient number of cellular solutions are presented. Therefore, the results for a solution at four different cell numbers were compared. The number of cells was 230,126 for a baseline, 650,640 cells for an intermediate, 3,678,622 for a good mesh, and 7,564,302 for a very good cellular decomposition.

The output temperature value obtained for the solution of each cellular model is shown in Figure 3. The results obtained for a good cellular model were considered to meet the requirements. In order to save computer memory and analysing time, a good cellular model with a cell number of 3,678,622 was selected and used in all subsequent calculations of the study.

3 Results and discussion

The results calculated from equations (1)–(4) were added to the analysis system as the main properties of the

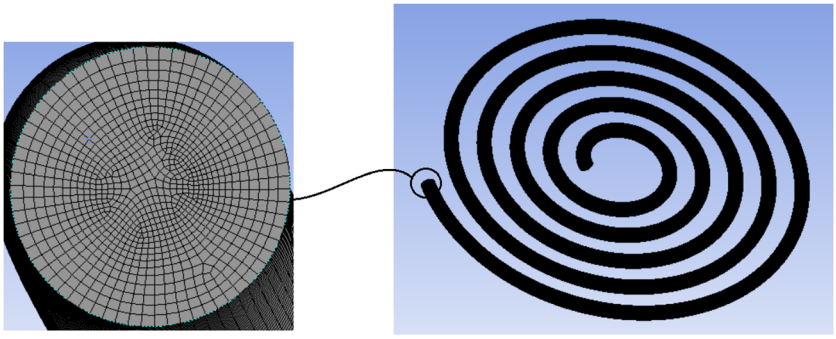

Figure 2: Finite element model.

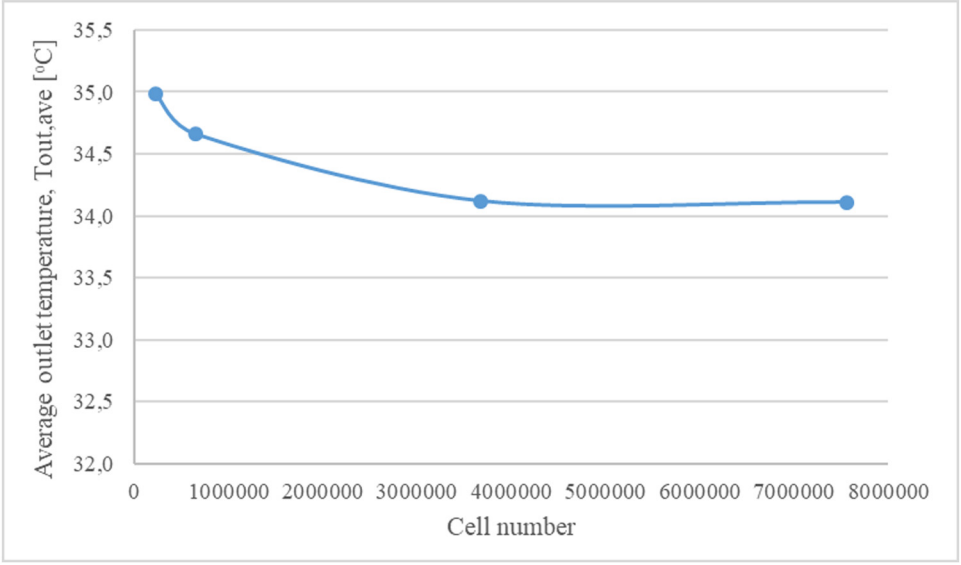

Figure 3: Mesh-independent test.

nanofluid. The laws of conservation of mass, momentum, and energy given in equations (5)–(8) were applied as the basis for calculations. Numerical calculations were performed at the initial and boundary conditions determined by considering the heat transfer expressions in fully developed internal flow conditions at constant surface temperature and compared with experimental studies and empirical expressions given in the literature.

Before presenting the results obtained for different fluids, it is reasonable to compare the results with those given in the literature for the base fluid, which is water, studied for the heat transfer evaluation along the spiral pipe. Such a comparison is shown in Figure 4. It can be realized that the Nusselt number increases with increasing Dean number for all cases. As can be seen from this comparison, which shows the Nusselt number values obtained according to the Dean number, quite consistent results were obtained with the literature.

Similarly, the friction factor values obtained from the analyses using water as a fluid were evaluated for geometries similar to those previously studied. Figure 5 shows such a comparison. As can be seen, the results are

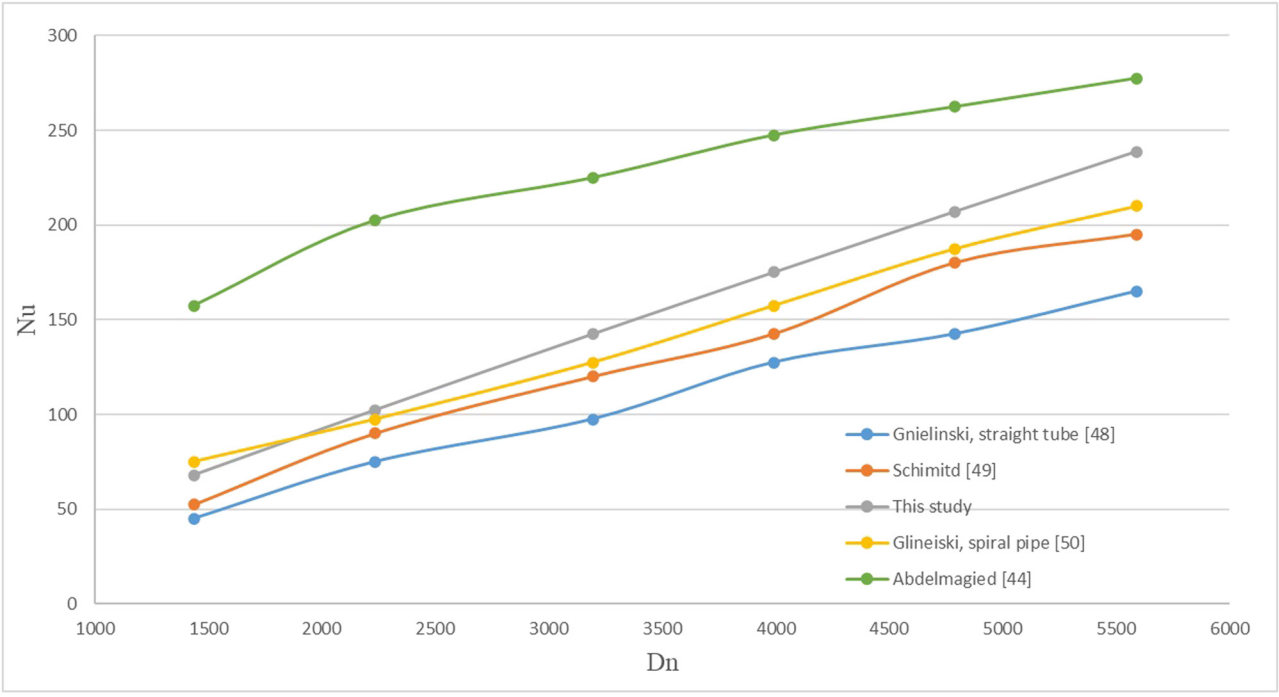

Figure 4: Comparison of Nu number for water flow in the spiral pipe.

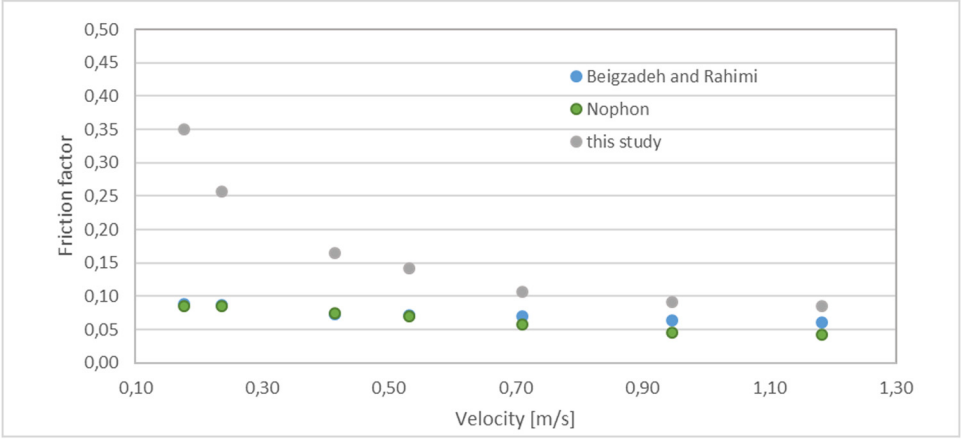

Figure 5: Geometry of the spiral pipe.

consistent with the values given by Beigzadeh and Rahimi [39] and Naphon [4].

3.1 Flow contours

The flow arrangements and parametric effects along the flow in the spiral tube are different from those in the planar tube. The largest role in this is played by the effect of centrifugal forces. The variation in velocity, pressure, and temperature, which are the basic parameters characterizing the flow, are responsible for the energy interactions throughout the flow. Therefore, they need to be evaluated separately. The influence of the difference in the radius of curvature of the spiral tube is also important. However, in this study, we considered a compact design of a spiral pipe with five turns and a curvature of 0.06. These property changes and effects explained below are valid for all nanofluids studied and are interpreted for specific numerical values on a single image.

Figure 6 shows the velocity change from the inlet to the outlet of the spiral model. At constant inlet velocity, a velocity gradient starts to form immediately after the inlet and before a quarter turn is made, and the velocity gradient that provides the developed flow conditions is reached.

The flow in the spiral flow is different from the maximum velocity at the centre in the straight pipe flow. Maximum velocity values are reached in the direction away from the centre of curvature along the progressive flow along the turn. This is also evident from the flow trajectories shown in Figure 7.

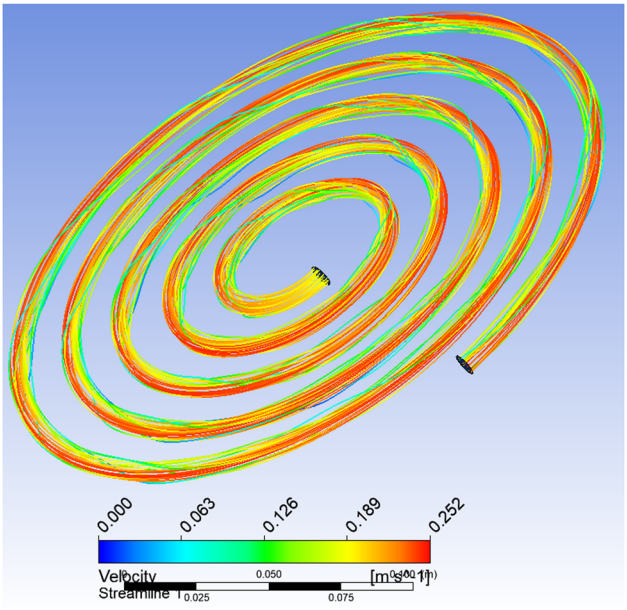

Figure 7: Velocity streamlines.

Figure 8 shows the pressure change from the inlet to the outlet of the spiral model. At a constant inlet velocity, a contour of decreasing pressure change from inlet to outlet is reached. In spiral flow, the flow shows a similar trend to the pressure drop in straight pipe flow. The presence of a secondary flow is observed under the influence of centrifugal forces caused by the curvature effect.

The temperature change in the flow model is shown in Figure 9. As expected, the regional average temperature values have an increasing effect from the inlet to the outlet.

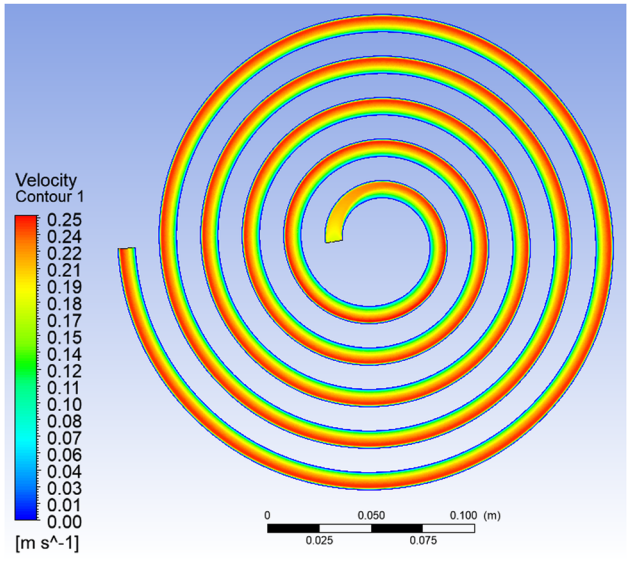

Figure 6: Velocity contours.

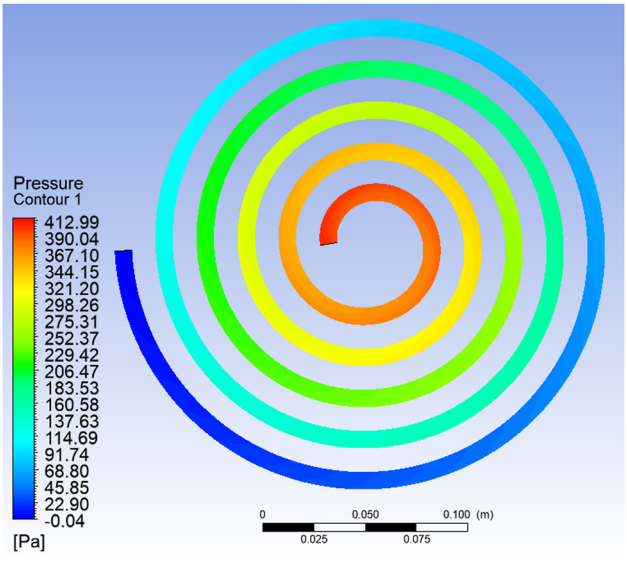

Figure 8: Pressure contours.

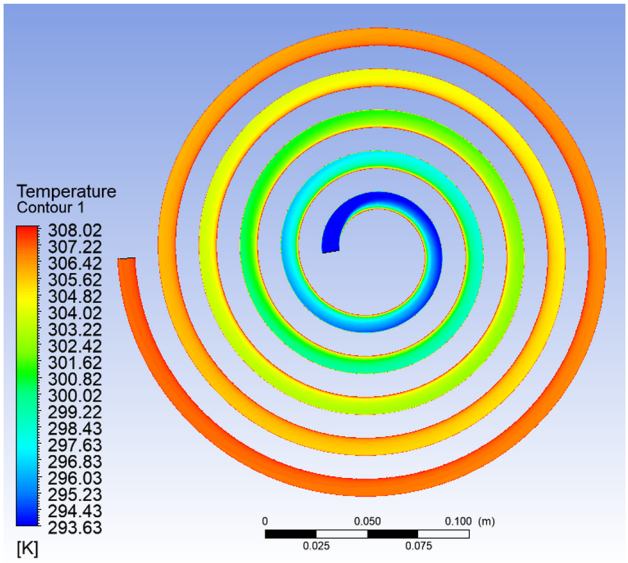

Figure 9: Temperature contours.

However, unlike the straight pipe flow, higher temperature values occur near the centre of curvature, where the velocity decreases along the cross section. In this way, the heat transfer intensity remains in the inner region near the centre of curvature. Taking into account that heat losses will increase as they approach regions outside the heating zone, this formation provides a useful heat transfer model for many applications.

The resulting parametric contours for the cross section of the flow model at the end of each rotation are shown in Figure 10 for five rotations separately. Thus, the changes from the centre of curvature outwards are clearly seen. The velocity, pressure, and temperature gradients are developed through a specific and systematic change. For such a velocity–pressure-based analysis, it was recognized that the heat transfer effect would be dominated by centrifugal forces up to a certain rotation.

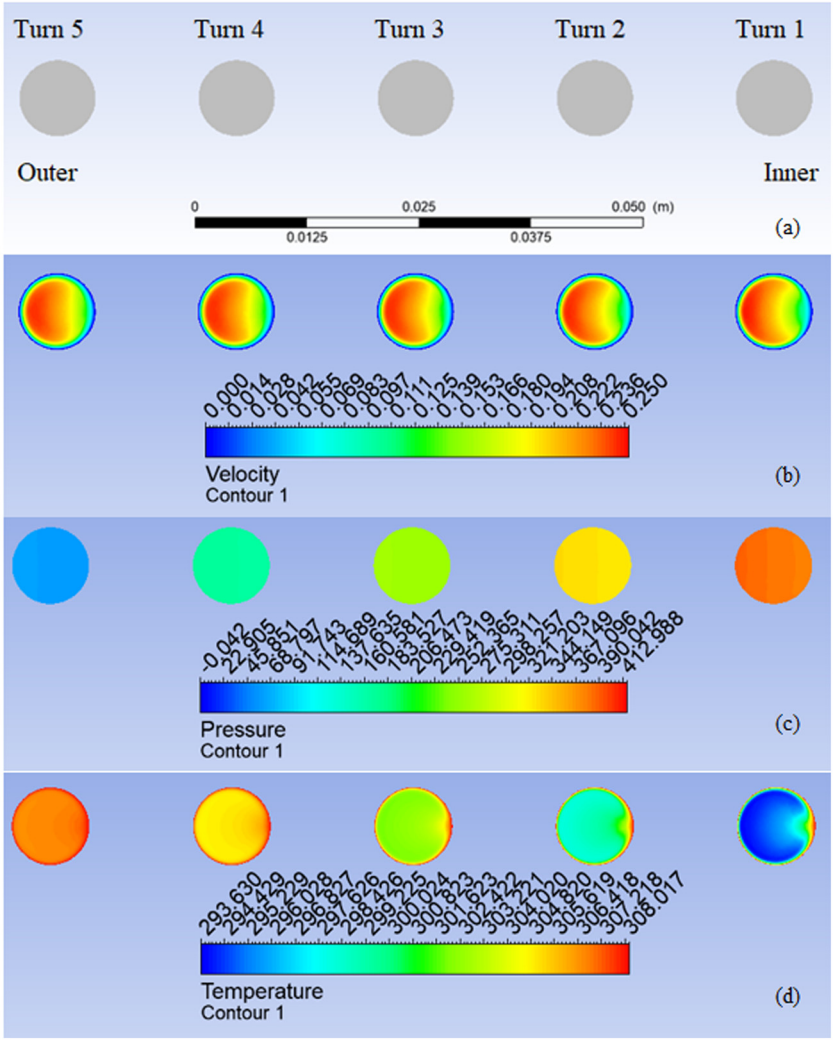

Figure 10: Cross section of the flow contours along the turns: (a) turn number, (b) velocity, (c) pressure, and (d) temperature.

3.2 Nanofluid effect

The calculated properties of the nanofluids with different volume concentrations (1–5%) are given in Table 3. These values were obtained by using equations (1)–(4) with the density, specific heat, and heat transfer coefficient values of water and nanoparticles given in Table 2. According to these calculated numerical values, the fluids were defined and solved separately in Fluent.

Figure 11 shows the average outlet temperature values (T_{out}) of water and the chosen nanofluids (TiO_2, Al_2O_3, Fe_2O_3, CeO_2, CuO, ZnO) for this study at different Reynolds numbers. As can be seen from the figure, water has the lowest outlet temperature value. It is seen that the lowest outlet temperature value of the nanofluids is in TiO_2, and the greatest outlet temperature value is in CeO_2. It was also found that the outlet temperature values decreased as the Reynolds number increased. This is because different nanoparticles have different thermodynamic properties like density, specific heat, and heat transfer coefficient.

Figure 12 shows the effect of the nanofluids with a volumetric concentration of 1% on the average heat transport coefficient at varying Re numbers. The secondary flow in the spiral tube is caused by centrifugal forces. Therefore, it leads to higher turbulence intensity and, consequently, an increase in the heat transfer rate. An increase in Re increases the turbulent effects. This increase remains valid for all types of nanofluids and has larger transport effects than water. As can be seen from Figure 12, water has a lower heat transfer coefficient value than the others. It is seen that the lowest heat transfer coefficient value of nanofluids is in TiO_2, and the highest heat transfer coefficient value is in CeO_2. This implies that different nanoparticles have different thermodynamic properties like density, specific heat, and heat transfer coefficient. The greater thermal conductivity of the nanoparticles and the decrease in the thickness of the thermal boundary layer are attributed to

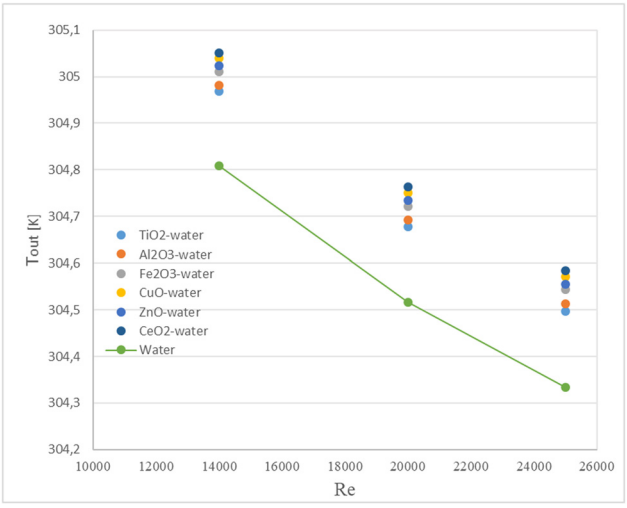

Figure 11: Outlet temperature values of water and different nanofluids at some Re values.

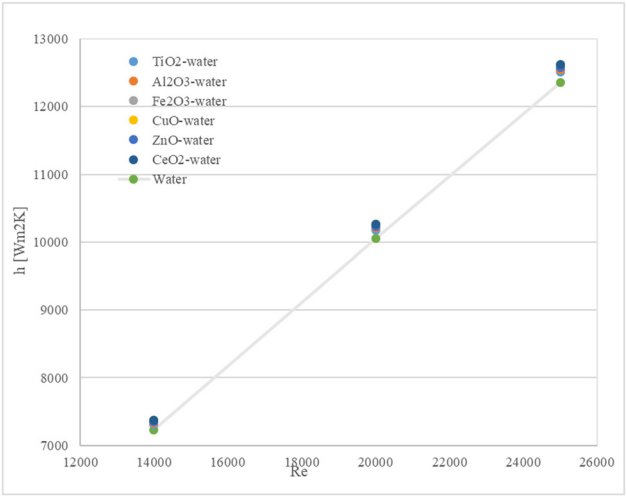

Figure 12: Heat transfer coefficient values of water and different nanofluids at some Re values.

Table 3: Computed nanofluid properties

Nanofluid	ρ [kg/m^3]			*Cp* [J/kg K]			*k* [W/mK]		
Volume concentration	1%	3%	5%	1%	3%	5%	1%	3%	5%
TiO_2–water	1029.63	1094.89	1160.15	3,934	3,676	3,447	0.7142	0.7432	0.7730
Al_2O_3–water	1026.03	1084.09	1142.15	3,955	3,731	3,719	0.7202	0.7617	0.8050
Fe_2O_3–water	1041.23	1129.69	1218.15	3,897	3,580	3,309	0.7182	0.7556	0.7943
CeO_2–water	1058.35	1181.05	1303.75	3,832	3,421	3,087	0.7179	0.7545	0.7924
CuO–water	1052.33	1162.99	1273.65	3,857	3,482	3,172	0.7189	0.7577	0.7980
ZnO–water	1041.63	1130.89	1220.15	3,888	3,557	3,275	0.7194	0.7594	0.8008

the increase in the convection heat transfer coefficient. This results in the momentum of the nanoparticles moving away from the wall and toward the centre of the tube, as well as a decrease in viscosity in the wall region. The thermal conductivity and specific surface area of nanoparticles are the main factors that influence how well nanofluids transmit heat. They have contributed to the increase in the coefficient of heat transmission.

The empirical relations developed for Nu and f [39] are given in equations (16) and (17). The correlation of the numerical h and Nu values obtained according to the nanofluid types with these equations is given in the relevant figures. As can be seen from the equations, the curvature ratio significantly affects both results.

$$\mathrm{Nu} = 0.359\,\mathrm{Re}^{0.781}\,\mathrm{Pr}^{0.016}\delta^{0.933}\gamma^{-0.172}, \tag{16}$$

$$f = 2.32\,\mathrm{Re}^{-0.311}\,\delta^{0.467}\gamma^{-0.074}. \tag{17}$$

Figure 13 demonstrates the value of the friction coefficient of water and the nanofluids at different Reynolds numbers. As can be seen from the figure, the coefficient of friction value of water is the highest. It can be observed that TiO_2 has the greatest coefficient of friction value among the nanofluids, whereas CeO_2 has the lowest. It was also found that the coefficient of friction values decreased as the Reynolds number increased. Increasing the boundary layer thickness reduces the friction factor. This decrease in the friction factor is caused by secondary flows due to centrifugal forces. Thus, higher viscosity reduces the friction factor. As the number of turns increases, the normalized friction factor tends to decrease towards straight pipe values.

Figure 14 demonstrates the average Nusselt number value of water and the nanofluids at a concentration of 1% by volume at different Reynolds numbers. As illustrated in the figure, the Nusselt number value of water is the lowest. It is seen that the lowest Nusselt number value of the nanofluids is in Al_2O_3, and the highest Nusselt number value is in CeO_2. It was also found that the Nusselt number values increased as the Reynolds number increased. Centrifugal force drives the fluid particles away from the tube's centre due to the secondary flow that develops along the flow, which speeds up the rate of heat transmission. This increase can be ascribed to the fluid's higher heat conductivity than water, as well as to the nanoparticles' centrifugal motion, particle migration, and thickness reduction of the boundary layer. The rate of heat transfer from the wall to the fluid is accelerated by the relative motion of nanoparticles near the wall [41,43]. This indicates that the tubes' curvature has a significant impact on how quickly heat is transferred through them. As Re increases, the resistance and the thickness of the thermal boundary layer both decrease thermally. Thus, the average amount of heat transfer coefficient increases. Turbulent flow increases the amount of heat transfer and friction factor. This is because the thermal boundary layer thickness along the flow path decreases with the increase in Re, which means that turbulence intensifies. The fluid's tendency to flow towards the pipe's exterior leads the centrifugal force along the spiral to turn significantly, altering the velocity profile, which in turn causes a partial decrease in the boundary layer's thickness. This secondary flow is a flow with radial velocity components that are perpendicular to the primary flow. Thus, the velocity for secondary flow increases and there is a greater mixing of the flows between the tube's core and the walls nearby.

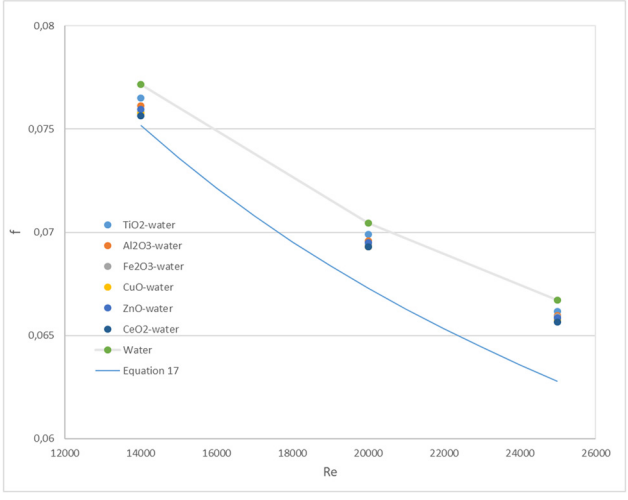

Figure 13: Friction factor change of water and different nanofluids at some Re values.

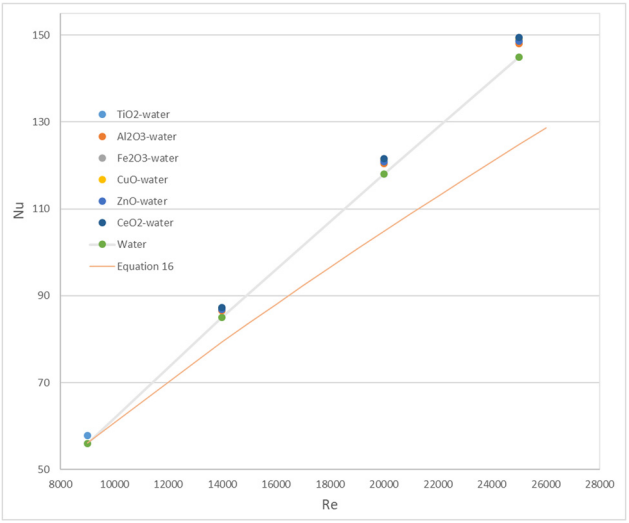

Figure 14: Nusselt number change of water and different nanofluids at some Re values.

4 Conclusions

This study investigates the heat transfer and flow behaviour of water and nanofluids flowing in a spiral-coiled tube. The Nusselt number, heat transfer coefficient, outlet temperature, and coefficient of friction values of different nanofluids such as TiO_2, Al_2O_3, Fe_2O_3, CeO_2, CuO, ZnO, and water at different Reynolds numbers were calculated and compared with each other. It was noted that the use of different types of nanofluids in the tube changes the fluid behaviour. At the same Reynolds number, the Nusselt number, heat transfer coefficient, outlet temperature, and coefficient of friction values were found to change when different types of nanofluids were used. Another reason for this is the secondary flow and rotating flow due to centrifugal forces. In addition, the coefficient of friction values f of water at different velocities were calculated and found to be consistent with previous studies. It was concluded that the outlet temperature, convection heat transfer, and Nusselt number values of the nanofluids were higher, and the friction coefficient value was lower compared to only the water flow. Among the nanofluids, CeO was found to have the highest outlet temperature, heat transfer coefficient, Nusselt number value, and the lowest friction coefficient value. TiO_2 was found to have the lowest outlet temperature (T_{out}) and heat transfer coefficient value, as well as the highest coefficient of friction value. Al_2O_3 was found to have the lowest Nusselt number value. In addition, the Nusselt number values were obtained at different Dean numbers (2200–8600) and found to be consistent with previous studies. In addition, the coefficient of friction values of water at different velocities (0.18–1.18) were obtained and found to be consistent with previous studies.

Funding information: This research received no external funding.

Author contributions: Merdin Danışmaz – original draft preparation, review experimental treatment and methodology, editing; Mesut Demirbilek – investigation and visualization, data curation, and formal analysis.

Conflict of interest: The authors declare no conflict of interest.

Data availability statement: The datasets generated during and/or analysed during the current study are available from the corresponding author on reasonable request.

Ethical approval: The conducted research is not related to either human or animal use.

References

[1] Ciofa M, Arini A, Liberto MD. On the Influence of gravitational and centrifugal buoyancy on laminar flow and heat transfer in curved pipes and coils. Int J Heat Mass Transf. 2015;82:123–34.
[2] Nobari MRH, Amani E. A numerical investigation of developing flow and heat transfer İn a curved pipe. Int J Num Methods Heat & Fluid Flow. 2009;19(7):847–73.
[3] Wang M, Zheng M, Wang R, Tian L, Ye C, Chen Y, et al. Experimental studies on local and average heat transfer characteristics in helical pipes with single phase flow. Ann Nucl Energy. 2019;123:78–85.
[4] Naphon P. Experimental investigation the nano fluids heat transfer characteristics in horizontal spirally coiled tubes. Int J Heat Mass Transf. 2016;93:293–300.
[5] Patil RH. Experimental studies on heat transfer to Newtonian fluids through spiral coils. Exp Therm Fluid Sci. 2017;84:144–55.
[6] Nema PK, Datta AK. Improved milk fouling simulation in a helical triple tube heat exchanger. Int J Heat Mass Transf. 2006;49(19–20):3360–70.
[7] Ji JD, Ge PQ, Bi WB. Numerical investigation of flow and heat transfer performances of horizontal spiral-coil pipes. Journal of Hydrodynamics. Ser B. 2016;28(4):576–84.
[8] Zou C, Zhang Y, Feng H, Falcoz Q, Neveu P, Gao W, et al. Effects of geometric parameters on thermal performance for a cylindrical solar receiver using a 3D numerical model. Energy Convers Manag. 2017;149:293–302.
[9] Hardik BK, Baburajan PK, Prabhu SV. Local heat transfer coefficient in helical coils with single phase flow. Int J Heat Mass Transf. 2015;89:522–38.
[10] Kim YI, Kim SH, Hwang YD, Park JH. Numerical investigation on the similarity of developing laminar flows in helical pipes. Nucl Eng Des. 2011;241(12):5211–24.
[11] Lee M, Kang T, Kim Y. Air-side heat transfer characteristics of spiral-type circular fin-tube heat exchangers. Int J Refrig. 2010;33(2):313–20.
[12] Li S, Cai W, Chen J, Zhang H, Jiang Y. Numerical study on the flow and heat transfer characteristics of forced convective condensation with propane in a spiral pipe. Int J Heat Mass Transf. 2018;117:1169–87.
[13] Bartwal A, Gautam A, Kumar M, Mangrulkar CK, Chamoli S. Thermal performance intensification of a circular heat exchanger tube integrated with compound circular ring–metal wire net inserts. Chem Eng Process – Process Intensif. 2018;124:50–70.
[14] Eiamsa Ard S, Wongcharee K, Kunnarak K, Kumar M, Chuwattabakul V. Heat transfer enhancement of TiO2-water nanofluid flow in dimpled tube with twisted tape insert. Heat Mass Transf. 2019;55(10):2987–3001.
[15] Verma A, Kumar M, Patil AK. Enhanced heat transfer and frictional losses in heat exchanger tube with modified helical coiled inserts. Heat Mass Transf. 2018;54:3137–50.
[16] Akhavan-Behabadi MA, Pakdaman MF, Ghazvini M. Experimental investigation on the convective heat transfer of nano fluid flow Inside vertical helically coiled tubes under uniform wall temperature condition. Int Commun Heat Mass Transf. 2012;39(4):556–64.
[17] Narrein K, Mohammed HA. Influence of nano fluids and rotation on helically coiled tube Heat exchanger performance. Thermochim Acta. 2013;564:13–23.
[18] Jamal-Abad MT, Zamzamian A, Dehghan M. Experimental studies on the heat transfer and pressure drop characteristics of Cu–water

and Al–water nano fluids İn a spiral coil. Exp Therm Fluid Sci. 2013;47:206–12.
[19] Naphon P, Arisariyawong T, Wiriyasart S, Srichat A. ANFIS for analysis friction factor and Nusselt number of pulsating nano fluids flow in the fluted tube under magnetic field. Case Stud Therm Eng. 2020;18:100605.
[20] Suresh S, Chandrasekar M, Sekhar SC. Experimental studies on heat transfer and friction factor characteristics of CuO/water nano fluid under turbulent flow in a helically dimpled tube. Exp Therm Fluid Sci. 2011;35(3):542–9.
[21] Sasmito AP, Kurnia JC, Mujumdar AS. Numerical evaluation of laminar heat transfer enhancement in nano fluid flow in coiled square tubes. Nanoscale Res Lett. 2011;6:376.
[22] Kannadasan N, Ramanathan K, Suresh S. Comparison of heat transfer and pressure drop in horizontal and vertical helically coiled heat exchanger with CuO/water based nano fluids. Exp Therm Fluid Sci. 2012;42:64–70.
[23] Hashemi SM, Akhavan-Behabadi MA. An empirical study on heat transfer and pressure drop characteristics of CuO–base oil nano fluid flow in a horizontal helically coiled tube under constant heat flux. Int Commun Heat Mass Transf. 2012;39(1):144–51.
[24] Jamshidi N, Farhadi M, Sedighi K, Ganji DD. Optimization of design parameters for nano fluids flowing inside helical coils. Int Commun Heat Mass Transf. 2012;39(2):311–7.
[25] Srinivas T, Vinod AV. Performance of an agitated helical coil heat exchanger using Al2O3/water nano fluid. Exp Therm Fluid Sci. 2013;51:77–83.
[26] Hasan MF, Danışmaz M, Majel BM. Thermal performance investigation of double pipe heat exchanger embedded with extended surfaces using nano fluid technique as enhancement. Case Stud Therm Eng. 2023;43:102774.
[27] Kahani M, Heris SZ, Mousavi SM. Multiwalled carbon nanotube/water nano fluid or helical coiling technique, which of them Is more effective? Ind Eng Chem Res. 2013;52(36):13183–91.
[28] Kahani M. Multiwalled carbon nanotube/water nano fluid or helical coiling technique, which of them is more effective? Ind & Eng Chem Res. 2013;52(36):13183–91.
[29] Khairul MA, Saidur R, Rahman MM, Alim MA, Hossain A, Abdin Z. Heat transfer and thermodynamic analyses of a helically coiled heat exchanger using different types of nano fluids. Int J Heat Mass Transf. 2013;67:398–403.
[30] Sasmito AP, Kurnia JC, Wang W, Jangam SV, Mujumdar AS. Numerical analysis of laminar heat transfer performance of İn-plane spiral ducts with various cross-sections at fixed cross-section area. Int J Heat Mass Transf. 2012;55(21–22):5882–90.
[31] Rahman MRA, Leong KY, Idris AC, Saad MR, Anwar M. Thermal fluid dynamics of Al2O3–Cu/water hybrid nanofluid in inclined lid driven cavity. J Nanofluids. 2017;6(1):149–54.
[32] Xuan Y, Li Q. Heat transfer enhancement of nano fluids. Int J Heat Fluid Flow. 2000;21(1):58–64.
[33] Sheikholeslami M, Sajjadi H, Delouei AA, Atashafrooz M, Li Z. Magnetic force and radiation influences on nano fluid transportation through a permeable media considering Al2O3 nanoparticles. J Therm Anal Calorim. 2019;136(6):2477–85.
[34] Mirfendereski S, Abbassi A, Saffar-avval M. Experimental and numerical investigation of nano fluid heat transfer in helically coiled tubes at constant wall heat flux. Adv Powder Technol. 2015;26(5):1483–94.
[35] Nassan TH, Heris SZ, Noie SH. A comparison of experimental heat transfer characteristics for Al2O3/water and CuO/water nano fluids in square cross-section duct. Int Commun Heat Mass Transf. 2010;37(7):924–8.
[36] Hassani M, Lavasani MA, Kim YS, Ghergherehchi M. Numerical investigation of nano fluid Al2O3/water in elliptical tube equipped with Ttwisted tape. Int J Heat Technol. 2019;37(2):520–6.
[37] Yoo GJ, Choi HK, Dong WR. Fluid flow and heat transfer characteristics of spiral coiled tube: Effects of Reynolds number and curvature ratio. J Cent South Univ. 2012;19(2):471–6.
[38] Malviya R, Baredar PV, Kumar A. Thermal performance improvement of solar parabolic dish system using modified spiral coil tubular receiver. Int J Photoenergy. 2021;18:1–18.
[39] Beigzadeh R, Rahimi M. Prediction of thermal and fluid flow characteristics in helically coiled tubes using ANFIS and GA based correlations. Int Commun Heat Mass Transf. 2012;39(10):1647–53.
[40] Seyedashraf O. Numerical study of pressure drop in the horizontal. Trak Univ J Eng Sci. 2015;16(2):55–60.
[41] Abdi H, Asaadi S, Kivi HA, Pesteei SM. A comprehensive numerical study on nano fluid fow and heat transfer of helical, spiral and straight tubes with different cross sections. Int J Heat Technol. 2019;37(4):1031–42.
[42] Huminic G, Huminic A. Heat transfer and fow characteristics of conventional fluids and nano fluids in curved tubes: A review. Renew Sustain Energy Rev. 2016;58:1327–47.
[43] Abdelmagied M. Thermal performance characteristics of a triple spiral tube heat exchanger. Chem Eng Process – Process Intensif. 2020;149:107707.
[44] Faisal KM, Mohammed BA. Design of nano fluid-based spring water/tap water and nanoparticles of Fe2O3/ZnO as a coolant for the engines. Diyala J Eng Sci. 2023;16(3):147–63.
[45] Stalin PMJ, Arjunan TV, Matheswaran MM, Kumar PM, Sadanandam N. Investigations on thermal properties of CeO2/water nanofluids for heat transfer applications. Mater Today: Proc. 2021;47:6815–20.
[46] Ramasamy D, Ramachandran SSR, Gunasekharan TS. Experimental analysis of thermal performance of solar collector using CuO-H_2O nano fluid. Int J Innovative Technol Explor Eng (IJITEE). 2018 (2S2):8.
[47] Versteeg HK, Malalasekera W. An introduction to computational fluid dynamics. Finite Vol Method. Edinburgh Gate, Harlow, England: Pearson Education Limited; 1995.
[48] Schmidt EF. Heat transfer and pressure loss in coils. Chem Ing Technic. 1967;39(13):781–9.